A Shapeshifting Ferrofluidic Robot

[a]Reza Ahmed, [a]Mahdi Ilami, [a]Joseph Bant, [a]Borhan Beigzadeh, [a]Hamid Marvi

[a]*School for Engineering of Matter Transport and Energy (SEMTE), Arizona State University, 501 E Tyler Mall, Tempe AZ 85287-6106, USA*

Abstract

To create a miniature shapeshifting robot capable of controlled movement, subdivision, regeneration, passage through small channels, engulfment of particles, object manipulation, and flow manipulation; a droplet of magnetically responsive ferrofluid is used. The ferrofluidic robot can achieve the aforementioned functions when both its position and shape are controlled using a custom electromagnetic field generation system. It is demonstrated that the proposed robot can perform these functions with sub-millimeter and sub-degree error. A robot having these capabilities can remotely perform medical and microassembly tasks requiring fine dexterity that are currently difficult or impossible.

Introduction

Medical technology is striving towards less invasive operations and procedures in order to benefit patients by providing shorter recovery times, decreased risk of infection, and reduced chance of complications.[1–3] Furthermore, with the rapid advancement of micro- and nano-fabrication technologies, the development of new microassembly processes is of great interest.

Several research groups have turned to bio-inspired micro and nano robotics to improve medical procedures that would normally require invasive surgeries and significant operation time.[4,5] These tiny robots have been developed for performing surgeries,[6] treating tumors in difficult to reach locations,[7] and delivering drugs to targeted areas.[8] However, none of these microrobots exhibit the characteristics of advanced dexterity as described above. Onoda *et al.* developed an amoeba-like, self-oscillating polymeric fluid with autonomous sol-gel transition that was capable of self motility but only through the generation of hydrostatic pressure in a capillary tube at speeds of, at a maximum, 0.35 mm/s.[9] Fusco *et al.* proposed flat, solid rectangular microrobots for drug delivery that can curl into a tubular shape for improved locomotion and stunted drug release, and then open up again to a rectangular shape for increased drug delivery after reaching a target location.[10] Huang *et al.* developed a rapid prototyping method to produce microrobotic swimmers inspired by bacteria and eukaryotes utilizing synthetic flagella to achieve a broad range of motility modes in Reynolds numbers similar to those found in active blood vessels.[11] These microswimmers were made of a biocompatible hydrogel and magnetic nanoparticles, and had two functions: they gave the microrobots their shape during the manufacturing process, and made them move and swim when an electromagnetic field is applied. The researchers used a rotating uniform magnetic field to drive the flagella and thus, the robot. One limitation of this design is that the robots are beholden to travel in a helical pattern determined by the shape of the flagella at creation, limiting the degrees of motion. Fusco *et al.* created and tested a shape changing robot made of hydrogel bilayers to facilitate drug delivery.[12] Their microrobot was magnetically actuated and capable of switching shape from a cylinder to a rectangular configuration under the presence of near-infrared light. Kummer *et al.* invented the Octomag, an 8 coil electromagnetic field generation system, and with a magnetic microrobot with a sharp needle attachment performed untethered blood vessel puncturing of a developing chicken embryo.[6]

The potential of ferrofluid droplets to be used as miniature soft robots has been explored by different research groups. Ferrofluid is a stable colloidal suspension of small ferromagnetic or paramagnetic particles dispersed in a surfactant to prevent agglomeration. The fluid properties of this material limit magnetic response to superparamagnetic behavior. That is, in the presence of an external magnetic field the magnetic moment of the individual ferromagnetic

particles in the material align with the magnetic field, producing an induced magnetic moment in the direction of the external magnetic field.[13,14] The magnetic forces arising therefrom, in combination with the containing force of surface tension, allow for the ferrofluidic robot as a whole to be manipulated via control of the external magnetic field. This superparamagnetism property, along with its liquid properties, makes ferrofluid well suited for a range of biomedical applications.[15,16] Research done by Komaee and Shapiro studied the movement of a ferrofluid droplet in a four-coil electromagnetic setup using a control equation based on a physical model of the magnetic and viscous forces on the ferrofluidic droplet.[17] They confirmed their model using both computational and experimental studies that demonstrated the position control; however, they did not attempt any shape control. Komaee and Shapiro, in further research with Probst *et al.* took the previous work another step forward by optimizing the control of ferrofluid in a two dimensional plane for minimal electrical power.[18] Another project by Ody *et al.* attempted to control the movement of ferrofluid using a combination of uniform magnetic field and hydrophilic aluminum and hydrophobic copper surfaces.[19] They could stop and "pin" a ferrofluid droplet from sliding on a surface of varying tensions. However, this method had the disadvantage of requiring a specialized surface with which to operate and could only function in one predetermined direction. Contrariwise, it has been recently demonstrated by Katsikis *et al.* that it is possible to control a non-magnetic droplet in magnetic carrier fluid, having potential for microfluidics and assembly.[20] This alternative approach is however limited to scenarios when the carrier fluid can be chosen as the magnetically responsive part.

Moreover, there have been studies into characterization and control of the shape and deformation of ferrofluid droplets under the presence of a magnetic field. In these previous works, however, control of droplet shape has relied on augmenting the droplet surface by the addition of capillary or chemically formed membranes. Liu *et al.* demonstrated a method of forming mechanically deformable ferromagnetic liquid droplets that retain some magnetization outside of a magnetic field. This reversible process was based on locking the small magnetic particles of a ferrofluid in a soft, plastically deformable outer layer of the droplet. The droplets formed in this way demonstrated the capability of flow manipulation via rotation, but were unable to split and recombine, or actively reshape under magnetic control only.[14] Jamin *et al.* investigated a method of capillary origami using a ferrofluid droplet. By using capillary membranes on the surface of the droplet, a unique shape was formed through the magnetic forces acting on the droplet-membrane assembly.[21] They discovered an instability in the shape when the magnetic field reached a critical strength that scales with the volume of ferrofluid used. This research focused on the height of the droplet/membrane assembly, this being the only metric by which shape control was identified. Furthermore, the droplet was confined to the dynamics of the origami membrane, and could not change shape arbitrarily once combined with the membrane. In another method of ferrofluid droplet shape control utilizing a membrane covered surface, Anjos *et al.* investigated the behavior of wrinkle and fold patterns that arose in membranes grown on ferrofluid droplets in response to applied magnetic fields.[22] Again, the existence of a membrane limited the droplet's capabilities to behave as a fluid. Furthermore, Varma *et al.* presented a study on the influence that a magnetic field had on the formation of ferrofluid droplets based on perimeter, aspect ratio, velocity, and inter droplet spacing in a microchannel for laboratory-on-a-chip purposes.[23] While this study did demonstrate a level of control over velocity and shape of a droplet, it did not attempt to control the direction or position of the droplet, and instead allowed it to follow the flow of the carrier fluid, limiting its use. Chen *et al.* investigated the formation and rotation of ferrofluid droplets under the presence of a rotating magnetic field.[24] They modeled a ferrofluid droplet as an ellipsoid and achieved ratios of major to minor axis ranging from 1.5 to 3.5. However, they did not attempt to simultaneously control position and shape of the droplet and thus could not have achieved advanced dexterity.

Modelling techniques for ferrofluid droplet shape in circumstances mirroring similar applications have

also been investigated. The behavior of a ferrofluid droplet subject to both shear hydrodynamic flow of a carrier fluid and magnetic forces due to an applied field has been explored by Cunha *et al.*, vital for medical applications involving dynamically flowing carrier fluids.[25] Zhu *et al.* reported experimental and numerical results for how a droplet of ferrofluid deforms under a uniform magnetic field. They studied the profile of the droplet on a superhydrophobic surface and then developed a three-dimensional numerical model to predict the deformation under different magnetic fields.[26] This research examined an immobile droplet and made no attempt to control it. Ghaffari *et al.* created a CFD model of a falling ferrofluid droplet[27] and confirmed it with experimental data from Afkhami *et al.*[28] They later expanded upon their previous work and added collisions to their model[29] using the experimental data from Qian and Law.[30] The work of Ghaffari *et al.* aligned well with the experimental data presented. Observation-based modelling of ferrofluid droplets is progressing; although applied control on the shape of the droplet has yet to be achieved, and may be needlessly complex. Despite all the efforts in this field and among all studies on ferrofluid droplets, none has sought to combine both shape and position control into one unified control scheme capable of manipulating the droplet with a high level of dexterity which considerably limits the possible applications.

Objectives

For a small scale liquid robot to assist with minimally invasive medical procedures and new microassembly processes, advanced dexterity – characterized by controlled mobility, deformation, splitting, recombination, squeezing through narrow gaps, engulfment or pushing of objects, and induction of local flow – is highly desirable.

Considering the potential of ferrofluid droplets as small scale soft robots to enable higher dexterity, we propose a miniature, deformable ferrofluidic robot, capable of controlled translation and shape change that can achieve the aforementioned maneuvers. The achievement of these functional maneuvers via the present research is conceptualized in Figure 1. Using a droplet of ferrofluid, all of these functions can be performed by carefully controlling the external magnetic field generated by the electromagnetic coil system shown in Supplementary Figure S1. In particular, we present the approach to control both position and shape of the ferrofluid droplet using either four or eight electromagnetic coils. Since the position control of ferrofluid droplets using external magnetic fields has been well studied, we focus on shape control and combined shape and position control of ferrofluidic droplets. Finally, by employing these functionalities, we demonstrate capabilities such as sorting particles and flow generation for microfluidic and lab-on-a-chip applications.

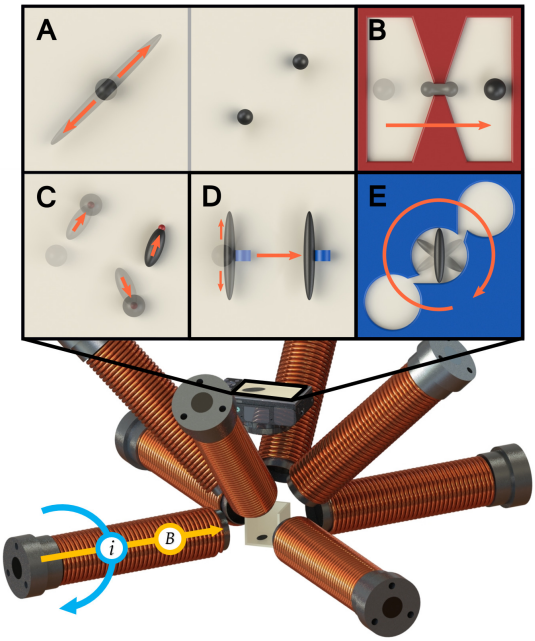

Figure 1: Conceptualization of the ferrofluidic robot. Electromagnetic coils generate controlled magnetic fields to produce five functional maneuvers: A) splitting of the robot into 2 smaller parts, B) squeezing through a small channel, C) engulfment/transport of wettable particles, D) pushing/manipulating non-wettable particles, and E) pumping/flow-manipulation in a fluidic channel.

Results and Discussion

To evaluate the performance of the control architecture, shape controller is verified in isolation, and then coupled with position controller for verification in a combined experiment. The shape control and combined position and shape control experiments quantify the capabilities of the the robot's control scheme and actuation system. Quantified results of these validation experiments precede subjective demonstrations of five functions: splitting and recombination, squeezing through small passages, engulfment of particles, pushing particles, and flow generation. These experiments on various functional maneuvers are presented as extensions of the control strategy. The goal of these experiments is to demonstrate complex maneuvers of interest that are made possible through the combination of the shape and position control scheme.

Shape Control

A key feature of our approach is the ability to control the shape of the ferrofluidic robot, defined by two parameters: the major axis radius of an ellipse imposed on the robot's silhouette, L (stretch length, mm); and the angle between that ellipse's major axis and the horizontal axis, θ (stretch angle, degrees). Shape control experiments demonstrate performance of the robot's stretch length and stretch angle control, as presented in Figure 3. Figure 3A plots the steady state performance of stretch angle control, showing mean experimental angle +/− one standard error and the specified angle in the case of utilizing only 4 coils. Figure 3B plots the same for the case of control using 8 coils. The results are notably similar. Average and maximum error over all steady state angle measurements during this experiment is 0.7° and 5.8°, respectively, in the case of 4 coil control; and 0.1° and 5.9°, respectively, in the case of 8 coil control. Images of the robot are included in the figure to visualize stretch angle control. Stretch length control capabilities are plotted in Figure 3C for seven different specified stretch length radii ranging from 1.7 mm to 4.4 mm. Experimental steady state mean stretch length +/− one standard error is plotted under the specified stretch length. Mean stretch length is calculated by taking the average of the stretch length over 100 frames during the experiment after the angle has settled. Average and maximum error over all steady state mean stretch length measurements is less than 0.1 mm which is the minimum resolution that can be measured with this setup, for both 4 and 8 coil control methods. Robot images visualize relative stretch length, and are not to scale with respect to any axis. The robot shape can be controlled at any position in the workspace, and to any stretch intensity up to the robotic droplet splitting.

The shape of a ferrofluid droplet is indeed enforced by the stresses acting on its boundary. Considering an inviscid, isothermal, and incompressible ferrofluid droplet surrounded by a nonmagnetic fluid, the balance of stresses at the boundary between the ferrofluid droplet and the surrounding fluid can be expressed using Equation 1[26,31] (Figure 2):

$$P^* + P_n = P_o + P_c. \tag{1}$$

In this equation, composite pressure (P^*) and fluid-magnetic pressure (P_m) are bulk pressures defined as $P^* = P(\rho, T) + P_m$ where $P(\rho, T)$ represents the thermodynamic pressure (ρ and T are the density and temperature of the ferrofluid) and $P_m = \mu_0 \int_0^H M dH$ (μ_0, H and M are the permeability of vacuum, the external magnetic field strength, and the corresponding magnetization of the ferrofluid, respectively). Furthermore, magnetic normal traction (P_n) and capillary pressure (P_c) are the interfacial force densities. $P_n = \mu_0 \frac{M_n^2}{2}$ where M_n is the normal component of the magnetization. $P_c = 2C\sigma$, where C is the curvature, and σ is the surface tension. Moreover, P_o is the pressure applied by the nonmagnetic fluid on the droplet boundary.

In Equation 1, the magnetic surface force density ($P_n + P_m$) indicates the contribution of the external magnetic field on the normal stresses at the interface of the ferrofluid droplet and its surrounding fluid. According to Supplementary Equation 10, the magnetization of the ferrofluid changes with the external magnetic field strength. This, in turn, alters both P_n and P_m and thus, impacts the pressures on the boundary. Besides, Equation 1 implies that with

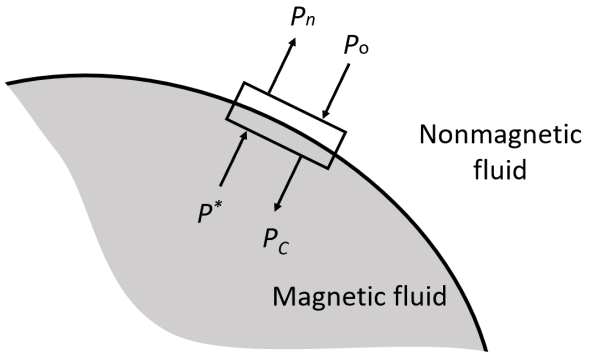

Figure 2: Balance of normal stresses at the interface of ferrofluid droplet and the surrounding fluid.

constant thermodynamic pressure and in a stationary surrounding fluid, the capillary pressure counterbalances the changes in magnetic surface force density. Since the surface tension of the ferrofluid in small magnetic fields can be considered constant,[32] the curvature of the boundary is the only factor responsible for changing the capillary pressure. Thus, by increasing the magnetic field strength, the curvature of the droplet boundary will change to balance the interfacial stresses. As changes in the magnetic surface force density are more significant at the points where the magnetization vector is normal to the boundary (along the magnetic field), the curvatures at those points experience larger variations. Hence, according to Supplementary Equation 12, the largest stretch occurs in the direction of the magnetic field (Supplementary Figure S2). In short, as the magnetic field strength increases, the droplet stretches along the direction of the magnetic field to balance the increased magnetic surface force density.

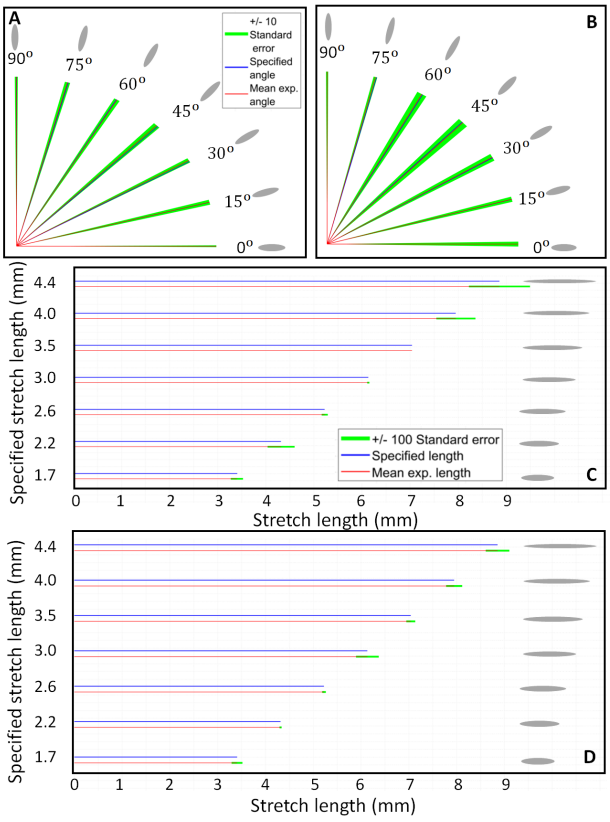

Figure 3: Shape control. Stretch angle (θ) and stretch length (L) for four-coil (A), (C) and eight-coil (B), (D) control methods, respectively. The specified stretch angle/length, experimental mean, and standard error of stretch angle and stretch length are plotted with blue lines, red lines, and green shades, respectively. The standard errors of stretch angle and stretch length are scaled 10 and 100 times, respectively, to make them visible. See Supplementary Video S1 for video footage of these experiments.

Combined Shape and Position Control

Position, stretch angle, and stretch length of the ferrofluid can be independently controlled by the magnetic field gradient, direction, and magnitude, respectively. Three independent proportional-integral-derivative (PID) controllers are used to control the ferrofluid droplet (Equations 2 and 3) and as a result, any combination of the position and shape can be achieved.

To demonstrate the ability to simultaneously control both position and shape, an experiment is performed in which the robot is tasked with following a specified path while holding specified stretch angles and lengths in four intervals. Results of this

experiment are presented in Figure 4, where mean experimental path +/− one standard error and specified path are plotted together. The robot follows the lemniscate path twice over the course of one experimental trial, and as such the figure is split into two parts for clarity. Figure 4A displays the mean experimental path +/− one standard error of the first half of the experiment, where the robot is set to a horizontal stretch angle and then to switch from one stretch length to a second stretch length after completing the first half of the lemniscate. Likewise, Figure 4B displays part two of the experiment where the robot is set to hold a vertical path and switch from a first stretch length to a second stretch length after completing the first half of the lemnsicate path. For these experiments, the position, the stretch angle, and the stretch length is controlled in closed loop. Data for this figure is taken over five experimental trials. Images of the ferrofluidic robot are underlaid beneath the plot to show the stretch angle and length changes over the course of the experiment. The average and maximum error of the experimental mean from the specified path for this experiment is 0.2 mm and 0.7 mm, respectively, for the 4 coil case; and 0.2 mm and 0.6 mm, respectively, for the 8 coil case.

Probst et al. performed position control of a ferrofluid droplet utilizing a four coil setup, and achieved errors ranging from 0.28 mm to 4.7 mm, for experiments with different sized droplets following straight, square, and spiral paths.[18] From the same research group, Komaee et al. performed a similar position experiment with simulation, where deviations from the desired path are reported visually.[17] The errors in position during path-following achieved in both studies are comparable with those achieved in the present study.

Although the eight coils control is singularity-free, the four coils control suffers from singularity when the stretch angle is 45 degrees (aligned with two coils). In this case, if the stretch angle needs to be maintained, the position control is only feasible along the major axis of the droplet (i.e. along the axis of the two coils the droplet is aligned with).

As can be seen in Figure 3, there are consistent deviations from the path. It may be due to the momentum that the droplet picks up as it accelerates during certain parts of the path. As velocity is not controlled, the actual velocity of the droplet may result in the droplet overshooting the desired point, between controller iterations. Increasing the control frequency would mitigate this issue. However, control frequency and resolution of the image for visual feedback are competing parameters: in order to increase the control frequency the image resolution would need to be reduced, and vice versa. Coupled improvement of image resolution and control frequency could be achieved by improving the computational power of the system used to run the control program.

Functional Maneuvers

As mentioned in the introduction, other researchers have used electromagnetic coil systems to manipulate either the position or the rotation and stretching of a ferrofluid droplet. However, none have manipulated a ferrofluid droplet's path while simultaneously controlling its shape.

Utilizing the position and shape control capabilities quantified above, the robot is capable of performing complex motions and functional maneuvers, namely: subdivision, regeneration, particle engulfment, particle sorting, and flow induction. Each maneuver is defined in terms of the robot's position, stretch length, and stretch angle, and performed in closed loop control. Successful performance of such tasks are demonstrated and visualized in Figure 5 and in Supplementary Video S1. All of these experiments are performed using only four coils.

Figure 5A demonstrates the robot's ability to split itself into separate parts and then recombine. The shape control scheme is applied to produce a short pulse at a specified stretch angle θ and at a very high stretch length M, such that the robot splits. Applying shape control at the same stretch angle but at a lower stretch length causes the smaller parts to contact one another, resulting in recombination via surface tension when allowed to return to rest. In Supplementary Video S1, splitting at two different angles is demonstrated.

The robot's ability to squeeze through a narrow channel is demonstrated in Figure 5B. To accomplish

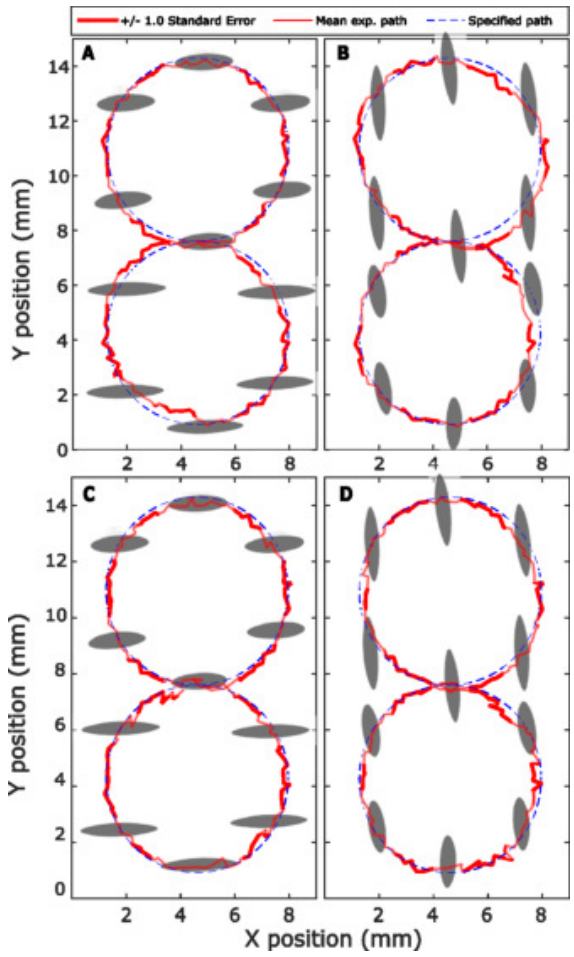

Figure 4: Combined position and shape control when following a lemniscate path. The lemniscate path is followed twice per experimental run: first holding a horizontal (A,C) and then a vertical (B,D) stretch angle at two stretch lengths. The specified path, experimental mean, and +/− one standard error are plotted with dashed blue line, solid pink line, and pink shade, respectively. Snapshots of the robot from corresponding time steps are overlaid on each plot. The size of these overlaid snapshots is reduced by half to improve visibility of the plots. See Supplementary Video S1 for video footage of these experiments.

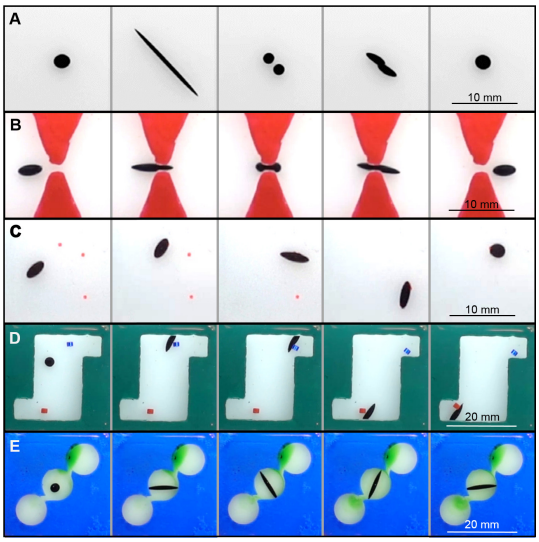

Figure 5: Functional maneuvers. A) closed-loop separation and recombination of the ferrofluidic robot emulating mitosis and regeneration, respectively. B) Closed-loop pulsing to squeeze through a channel. C) Particle engulfment experiment utilizing closed-loop position control to engulf and transport smaller particles. D) Closed-loop position and shape control to interact with/push particles to target locations. E) Closed-loop shape control to generate flow in a microfluidic channel. See Supplementary Video S1 for video footage of these experiments.

this task, the closed-loop position control scheme is used to move the robot to the channel entrance, then a directed pulsing motion is induced by combining the position control scheme with automated pulsing shape control signals. This pulsing action allows the robot to make incremental progress as it squeezes itself through the channel. The channel opening is 1 mm at its narrowest point. The robot can also be moved through a narrow channel by increasing the stretch length without pulsing shape control; however, depending on the channel width, it may result in splitting due to a large aspect ratio and the resisting forces applied by the channel edges.

As is demonstrated in the image sequence in Figure 5C, the robot can successfully "hunt" and en-

gulf wettable colored particles. When the ferrofluid droplet used in this study is submerged in isopropyl alcohol, glass and polished acrylic are considered as non-wettable, while polyethylene and most other plastics are wettable materials. The colored particles used in this experiment are wettable polymer beads (Cospheric Innovations UVPMS-BR-1.20 Fluorescent Red Polyethylene Microspheres) placed in the workspace randomly. The positions of the particles are obtained optically at the beginning of the experiment. This demonstration utilizes a combination of the position control scheme described earlier and a colored particle detection and tracking subprogram. The robot follows a path in closed loop which sequentially passes through the colored particles in a chosen order. The robot carries the engulfed particles as it continues along its path to engulf subsequent particles. This effectively accomplishes clearing the workspace and transporting the particles to the robot's end location. It is, however, observed that the robot becomes less responsive to the actuating magnetic field after gathering multiple particles. This may be due to the ferrofluid carrying extra weight that does not contribute to its magnetic properties. It is important to note that this functional maneuver is only achievable with particles that are wettable by the ferrofluid.

In Figure 5D, the robot is shown completing a task in which it must push two colored particles into separate target areas. This demonstration utilizes position only control to place the robot to the side of the particle in preparation to push, then uses a combination of shape and position control to push the particle into the target zone. The particles are colored glass cylinders of 1.3 mm diameter and 1.6 height. Glass is chosen as it is not wettable by the ferrofluid in 70% isopropyl alchohol. In addition, cylindrical particles are chosen for ease of pushing due to reduced friction through rolling. It is important to note that, in contrast to the engulfment maneuver, manipulation and sorting are only achievable for particles that are not wettable by the ferrofluid.

As shown in Figure 5E, flow can be induced in a microfluidic channel by controlling the the robot's shape. This experiment utilizes close-loop shape control only, maintaining stretch length and manipulating stretch angle incrementally to produce a rotary pump like mechanism. The microfluidic pump in Figure 5E is designed with three chambers; one to hold colored dye to visualize flow (top), one to contain the robot (mid), and the last containing only the carrier fluid to qualify flow (bottom). Two channels connect the three cells and are designed as nozzles/diffusers oriented to bias flow in the desired direction. The channel designs are based on a microfluidic pulse pump designed by Kawun *et al.*[33] The channels are also oriented to take advantage of the robot's rotation. A schematic of the rotational pump design is presented in Supplementary Figure S3.

Materials and Methods

The Experimental Setup

An electromagnetic field generation system is used to produce and manipulate the actuating magnetic field.[6] Eight stationary current controlled electromagnetic coils are used in the setup (Supplementary Figure S1): four arranged in-plane horizontally, equiangular around the workspace and facing inward; and the remaining four coils staggered 45 degrees both around the workspace and up towards the top of the workspace, with each coil facing downwards at a 45 degree angle towards the workspace. Each coil is composed of a solid iron core and 712 wraps of 14 gauge copper wire in 6 layers. The system is calibrated to 27 points comprising 8 "octants" within a $32 \times 32 \times 35$ mm^3 workspace cube. This calibration accounts for the linear relationships between each coil's magnetic field intensity and the robot's physical positioning in the workspace, thus allowing each coil to affect the robot predictably regardless of the robot's location.

Two power supplies are used; a TITAN F1208 capable of providing 60 A and up to 1200 W of electrical power, and an eFueld PSU50A V2 capable of providing 50 A and up to 1200W of electrical power. Four Sabertooth 2X25 dual motor drivers are used as amplifiers between the power supplies and the coils. Amplifiers are connected to a Sensoray Multifunction analog/digital I/O – Model 826 data acquisition card

(DAQ) to receive the controlling inputs. To avoid the adverse impacts of fluctuating temperatures on the magnetic field generation capabilities of the electromagnetic coils, a Fluid Chillers Inc. NEMA 4X Outdoor Enclosure cooling system circulates chilled water through copper tubing that is wound around each coil. While running this cooling setup, system temperatures remain between 21°C and 24°C.

The workspace is comprised of an open-top cube assembled from matte finished white acrylic square tiles, laser cut for repeatability and assembled via superglue, and a 3D printed white PLA fixture that holds the cube in place and acts as a sliding handle for inserting the cube into the center of the electromagnetic coil system. The cube is filled with 30 ml of 70% isopropyl alcohol; then 5 μL of the ferrofluid is added via micro pipette, forming a droplet.

In this study, only one ferrofluid (EFH-1) is explored. However, other ferrofluids will likely behave similarly as they all are colloidal suspensions of magnetic particles, regardless of particle size and suspension fluid. There are many types of ferrofluid with different properties, some of which are bio-compatible. EFH-1 ferrofluid is chosen for this study since it is found immiscible in 70% isopropyl alchohol, a commonly available substance. The scalability of ferrofluid droplet size is dependent upon the competing forces acting on it. The surface tension and cohesive forces work to bring the droplet into a spherical shape while magnetic forces attempt to deform it. The surface tension forces act on the surface while magnetic forces are body forces. Thus, the bigger the droplet gets (centimeter scale), the smaller the surface tension becomes compared to the magnetic forces which makes it difficult to keep the droplet together while applying magnetic forces. On the other hand, the surface tension becomes dominant in smaller droplets (micro scale) which forces the droplet into a spherical shape.

One stationary camera provides visual feedback of the workspace from the top. The camera is programmed to capture frames of 276 $\times$ 280 pixels, of which the ferrofluid's range of motion spans a 240 $\times$ 240 pixel region. Resolution is reduced to increase frame rate by reducing image processing computation time. The entire system is controlled through C++ by a single Dell Precision T1700 computer.

Control of the Robot's Position and Shape

One approach for controlling the position and shape of the ferrofluidic robot is to find a dynamic model of the droplet interacting with the environment as well as the magnetic fields and design a model-based controller for it. This model would be required to capture complex dynamics usually described by a set of partial differential equations, which in most cases may not be solved analytically.[34,35] Even for the cases that the analytical solution could be obtained, it is still required to solve the inverse problem to find the required currents of the coils for every desired position and shape of the robot. Furthermore, physical terms found in such a model need to be observed or estimated for each control loop iteration. To bypass the unnecessary complexity, computational cost, and time delay issues, a model-free controller is designed to control the position and shape of the robot. This controller has to withstand disturbances and uncertainties, and requires feedback information. Here, visual feedback is used to get the real-time information of the robot. By processing the feedback images, information about the position and shape of the robot is computed and provided to the controller.

The first step in defining the control problem is to standardize the robot's shape definition. If we do not apply abrupt changes to the resultant magnetic field, to a very good approximation, the robot can be modelled as an ellipsoid.[24,36] The projection of this ellipsoid onto a plane crossing its center parallel to the horizon is an ellipse in 2D, which can be easily seen from the camera installed above the workspace. This ellipse and its corresponding parameters are used to characterize the position and shape of the robot. It is worthy to note that the robot shape in 2D is determined using two parameters: the length of the ellipse major axis radius, L (stretch length), and its orientation, θ (stretch angle). The position of the robot is defined as that of the ellipse center point specified using two variables, P_x and P_y. Thus, assuming the robot has constant volume and that we do not apply intense and instantaneous magnetic field changes,

four variables are needed to completely describe the shape and position of the robot.

The electromagnetic field generation system can be used for controlling the above mentioned four variables through a multi-input-multi-output (MIMO) controller.

The proposed architecture for the controller is composed of 3 PID controllers: a controller on position composed of two identical PID controllers manipulating magnetic field gradient to control the dropet position, a PID controller on the magnetic field direction to control the ferrofluid droplet's stretch direction, and lastly, a PID controller on the magnitude of the magnetic field to control the ferrofluid droplet's stretch length. These controllers are all closed loop, relying on visual feedback to maintain control. The feedback loop uses the captured images of the workspace to compute four variables: P_x, P_y, L, and θ as described in the following section. Finally, the outputs of these three blocks are processed through an equation relating the currents within the electromagentic coils to the desired magnetic field and gradient at the position of the droplet. This relationship is solved to obtain the required current values for either 4 or 8 coil control, composing the final controller command sent to the coils.

To control the position of the robot, the position error vector, $\mathbf{E}_P$, of the desired location, $\mathbf{P}_d$, with respect to the current position of the robot, $\mathbf{P} = (P_x; P_y)$, is calculated as $\mathbf{E}_P = \mathbf{P}_d - \mathbf{P}$. The resultant force acting on the robot should be toward the desired location; that is, the direction of $\mathbf{E}_P$. The forces applied on the ferrofluid droplet in the x and y directions are defined by the $\mathbf{F}_{desired}$ terms in Equation 4. In fact, these are the variables that the position PID controllers are programmed to manipulate to achieve the desired location.

The electromagnetic field generation setup is designed with the intention that the magnetic field generated by each coil is in the linear regime over the entire workspace. Due to the relative sizes of the electromagnetic coils and the workspace, the magnetic field lines for each coil are nearly parallel to its axis. However, a thorough calibration process in which the field and gradient contributions of each coil at different current values are tabulated is necessary

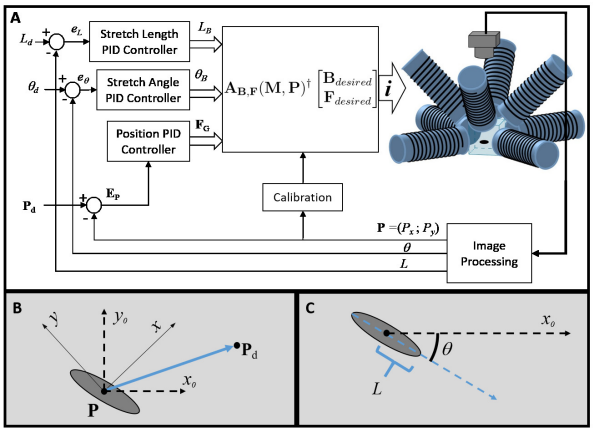

Figure 6: A) Control architecture of the ferrofluidic robot. L_d, θ_d, and $\mathbf{P}_d$ are the desired stretch length, stretch angle, and position. Errors for each parameter e_L, e_θ, and $\mathbf{E}_P$, act as inputs to their respective controllers. The controller outputs, L_B, θ_B, and $\mathbf{F}_G$ are the stretch length, stretch angle, and forces that need to be applied to the ferrofluid droplet so it can transition to the desired location and shape. These outputs are input to Equation 4, which relates these output parameters to current in the coils. Feedback parameters are collected via computer vision. B) Definition of position control parameter as the vector error between current robot position $\mathbf{P}$ and desired position $\mathbf{P}_d$ in a frame of reference xy rotated 45° from the image frame of reference x_0y_0. C) Definition of shape control parameters θ and L as the stretch angle and stretch length of the robot.

to accurately calculate the required currents. The force needed to act on the robot to move it towards the desired position can be written as:

$$\mathbf{F} = \begin{bmatrix} F_x \\ F_y \end{bmatrix} = \mathbf{K}_{PP}\mathbf{E}_P + \mathbf{K}_{DP}\dot{\mathbf{E}}_P + \mathbf{K}_{IP}\int \mathbf{E}_P dt \quad (2)$$

where $\mathbf{K}_{PP}$, $\mathbf{K}_{DP}$, and $\mathbf{K}_{IP}$ are three positive constants representing the proportional, derivative, and integral gains of the controller, tuned manually.

While the robot does not move under zero resultant force, it can be stretched proportional to and in the direction of, the magnetic field vector. In particular,

magnitude, L_B, and angle, θ_B, of the magnetic field vector determine the magnetization of the individual internal particles within the droplet, and thus the intensity to which the droplet is caused to align with the magnetic field. Therefore, to control the shape of the robot, the angle and intensity of the magnetic field is defined in terms of the errors in stretch angle, e_θ, and stretch length e_L.

$$\begin{aligned} \theta_B &= K_{P\theta} e_\theta + K_{D\theta} \dot{e}_\theta + K_{I\theta} \int e_\theta dt, \\ L_B &= K_{PL} e_L + K_{DL} \dot{e}_L + K_{IL} \int e_L dt, \end{aligned} \tag{3}$$

where $K_{P\theta}$, $K_{I\theta}$, $K_{D\theta}$, K_{PL}, K_{DL}, and K_{IL} are positive constants representing the proportional, derivative, and integral gains of the controllers, tuned manually. The gains of the controllers are as follows: for the position controllers, $K_{PP} = 0.5$, $K_{IP} = 0.002$, $K_{DP} = 0.1$; for the controller on the stretch length of the droplet, $K_{PL} = 0.08$, $K_{IL} = 0.02$, $K_{DL} = 0.02$; and lastly, for the controller on the stretch angle of the droplet, $K_{P\theta} = 0.5$, $K_{I\theta} = 0.05$, $K_{D\theta} = 0.5$. As with all controllers, the response of the system can be tuned to fit a desired behavior by altering these gains. The gains presented in this study were tuned specifically for the experiments. It is known that ferrofluid gets stretched along its magnetization vector which is always aligned with the external magnetic field. By applying control on the magnetic field direction, the stretch angle and magnitude can be controlled.

Magnetic field direction can be used to define the desired stretch angle. The magnetization of the ferrofluid is proportional to the external magnetic field acting on the ferrofluid. The applied magnetic gradient and the magnetization of the ferrofluid determine the force applied on the ferrofluid.

The electrical current in each coil to generate the required magnetic field and gradient can be determined considering the linear relation of magnetic field and electrical current. The net magnetic flux density and gradient can be calculated using the linear superposition of each electromagnetic coil's magnetic flux density and gradient contribution. As eluded to earlier, the contribution of each coil is measured through a calibration process for 1 A current. The required current ($i_0 ... i_7$) to achieve the desired forces and magnetic field can be calculated as,

$$\begin{bmatrix} i_0 \\ \vdots \\ i_7 \end{bmatrix} = \begin{bmatrix} \boldsymbol{\beta}(\mathbf{P}) \\ (\mathbf{M}(\boldsymbol{\beta}(\mathbf{P})))^T \boldsymbol{\beta}_x(\mathbf{P}) \\ (\mathbf{M}(\boldsymbol{\beta}(\mathbf{P})))^T \boldsymbol{\beta}_y(\mathbf{P}) \\ (\mathbf{M}(\boldsymbol{\beta}(\mathbf{P})))^T \boldsymbol{\beta}_z(\mathbf{P}) \end{bmatrix}^\dagger \begin{bmatrix} \mathbf{B}_{desired} \\ \mathbf{F}_{desired} \end{bmatrix}, \tag{4}$$

$$\begin{bmatrix} i_0 \\ \vdots \\ i_7 \end{bmatrix} = \mathbf{A}_{\mathbf{B},\mathbf{F}}(\mathbf{M}, \mathbf{P})^\dagger \begin{bmatrix} \mathbf{B}_{desired} \\ \mathbf{F}_{desired} \end{bmatrix}, \tag{5}$$

where $\boldsymbol{\beta}$ represents the magnetic field contribution of each of the eight electromagnetic coils at a particular position $\mathbf{P}$. $\boldsymbol{\beta}_x$, $\boldsymbol{\beta}_y$, $\boldsymbol{\beta}_z$ are the gradients of the calibration matrix in each direction at the position $\mathbf{P}$, $\mathbf{B}_{desired}$ is the flux density in each direction, $\mathbf{F}_{desired}$ is the desired force in each direction, $\mathbf{M}$ is the magnetization vector of the ferrofluid droplet under influence of a particular magnetic field, and † represents the pseudo-inverse (see Supplementary Text). For this application, the magnetization vector $\mathbf{M}$ is assumed to be a unit vector in the direction of $\mathbf{B}_{desired}$. This assumption is made in the case of rigid magnetic robots as well, and has been proven in past research to be a viable choice towards control of magnetic bodies in electromagnetic field generation systems such as the one used in this research.[6]

Control Scheme

To control the position and shape of the ferrofluid on a predetermined trajectory, the desired path and evolution is segmented into a series of steps which include a point-to-point breakdown of the desired path, required stretch angles, and required stretch lengths, fed to the controller in the form of an array. Each row in the array has four components corresponding to the x position, y position, stretch angle, and stretch length of the next desired pose. The magnetic field and gradient are controlled by PID controllers to steer the ferrofluid towards the next comprehensive pose in the array. As the droplet approaches the desired configuration, and falls within a predefined threshold of accuracy for each of the four metrics,

the controller will move on to the next point in the path, methodically moving through each predefined position/shape path.

Feedback Parameter Acquisition

The camera collects one top-view image of the workspace during every iteration of the experiment loop. The ferrofluidic robot appears black against a white background, making it very easy to threshold the image into a binary format. This thresholding process results in a binary image: an array of booleans marking only the pixels hosting the ferrofluidic robot. From this binary image, the center point of the droplet is obtained by the moments method in the OpenCV image processing library for C++. This method finds the "centroid" of the image by taking a weighted average of the pixel values in the x and y directions and dividing by the area of nonzero pixels. This method is effective for binary images, in particular.

The droplet's contours are determined from the binary image using the Canny method in OpenCV for C++. The Canny method is based on an edge detection algorithm invented in 1987 by John F Canny, and is a built-in function of the OpenCV library.[37] The contours are an array of Cartesian pixel coordinates that describe the outer boundary of the droplet. If multiple contours are detected in the image, all contours are combined into a single array and duplicate pixels in that resulting array are removed. This final array of pixels is used to determine the shape information by the following approach: The stretch angle, θ, is determined by finding the eigenvector that corresponds to the largest eigenvalue of the covariance matrix of all pixels comprising the boundary contour. The angle between this vector and the x_0 axis gives θ, as seen in Figure 6C. The other eigenvector describes the orientation of the droplet's minor axis, and is unused. The stretch length L is determined by finding the maximum distance from any contour pixel to the center point; resulting in a measurement of the major axis radius, as seen in Figure 6C.

Conclusion

Using an electromagnetic coil system, a control scheme is adapted for actuating a ferrofluid droplet robot in simultaneous position and shape control. The system uses visual feedback with closed loop control on position in x and y, stretch length, and stretch angle. Precision in the shape control and combined shape and position control of under 1 mm was demonstrated for all experiments. Five functional maneuvers are presented to illustrate the potential utility of the robot's advanced dexterity. The presented combination of actuation and control of a ferrofluid droplet robot is thus presented as a system for further research, with potential application in medical and microassembly processes.

In general, rigid robots may present higher accuracy in position and orientation control compared to ferrofluidic robots or other types of soft robots. However, some of the interesting functionalities offered by such soft robots (e.g. splitting, recombination, squeezing through narrow gaps, and particle engulfment) may not be readily achieved by their rigid counterparts. Achieving such dexterous functionalities are the main motivation behind this study, but additional efforts need to be made to further improve the accuracy and precision in control of the proposed ferrofluidic robot.

Additionally, many other exciting possibilities remain to be investigated. Control of position and shape in three dimensions is the logical next step following this research, and would enhance the effectiveness and adaptability of the robot in potential applications. Furthermore, a system and control scheme capable of controlling the shape and position of multiple robots independently would also be of great interest and thus, another potential direction for future research.

Acknowledgements

The authors would like to acknowledge Michael Kintscher for helping with development of the magnetic coil system, Edward Faillace for contributing to some of the experiments, Kenro Kusumi, Rebecca

Fisher, and Spring Berman for fruitful discussions about bio-inspired ferrofluidic robots, Paolo Velcich for permission to use a CAD camera model asset for creation of the Figure 1, and Arizona State University for financial support.

Author Disclosure Statement

No competing financial interests exist.

Supplementary Material

Supplementary Text
Supplementary Figure S1
Supplementary Figure S2
Supplementary Figure S3
Supplementary Video S1

References

[1] Nelson BJ, Kaliakatsos IK, Abbott JJ. Microrobots for minimally invasive medicine. Annual review of biomedical engineering. 2010;12:55–85.

[2] Burgner-Kahrs J, Rucker DC, Choset H. Continuum robots for medical applications: A survey. IEEE Transactions on Robotics. 2015;31(6):1261–1280.

[3] Ilami M, Ahmed RJ, Petras A, et al. Magnetic needle steering in soft phantom tissue. Scientific reports. 2020;10(1):1–11.

[4] Nelson BJ, Kaliakatsos IK, Abbott JJ. Microrobots for minimally invasive medicine. Annu Rev Biomed Eng. 2010;12(1):55–85.

[5] Bogue R, Troccaz J. The development of medical microrobots: a review of progress. Ind Rob. 2008; 35(4):294–299.

[6] Kummer MP, Abbott JJ, Kratochvil BE, et al. Octomag: An electromagnetic system for 5-dof wireless micromanipulation. IEEE Trans Robot. 2010; 26(6):1006–1017.

[7] Hajba L, Guttman A. Circulating tumor-cell detection and capture using microfluidic devices. Trends Analyt Chem. 2014;59:9–16.

[8] Steager EB, Sakar MS, Magee C, et al. Automated biomanipulation of single cells using magnetic microrobots. Int J Rob Res. 2013;32(3):346–359.

[9] Onoda M, Ueki T, Tamate R, et al. Amoeba-like self-oscillating polymeric fluids with autonomous sol-gel transition. Nat Commun. 2017;8:15862.

[10] Fusco S, Huang HW, Peyer KE, et al. Shape-switching microrobots for medical applications: The influence of shape in drug delivery and locomotion. ACS Appl Mater Interfaces. 2015;7(12):6803–6811.

[11] Huang HW, Sakar MS, Petruska AJ, et al. Soft micromachines with programmable motility and morphology. Nat Commun. 2016;7:12263.

[12] Fusco S, Huang HW, Peyer KE, et al. Shape-switching microrobots for medical applications: The influence of shape in drug delivery and locomotion. ACS Appl Mater Interfaces. 2015;7(12):6803–6811.

[13] Dreyfus R. An attractive, reshapable material. Science. 2019;365(6450):219–219.

[14] Liu X, Kent N, Ceballos A, et al. Reconfigurable ferromagnetic liquid droplets. Science. 2019; 365(6450):264–267.

[15] Huang G, Li M, Yang Q, et al. Magnetically actuated droplet manipulation and its potential biomedical applications. ACS Appl Mater Interfaces. 2017;9(2):1155–1166.

[16] Ilami M, Ahmed RJ, Edwards D, et al. Magnetically actuated tunable soft electronics. ACS omega. 2019;.

[17] Komaee A, Shapiro B. Steering a ferromagnetic particle by magnetic feedback control: Algorithm design and validation. In: *Proceedings of the 2010 American Control Conference*. 2010; 6543–6548.

[18] Probst R, Lin J, Komaee A, et al. Planar steering of a single ferrofluid drop by optimal minimum power dynamic feedback control of four electromagnets at a distance. J Magn Magn Mater. 2011; 323(7):885 – 896.

[19] Ody T, Panth M, Sommers AD, et al. Controlling the motion of ferrofluid droplets using surface tension gradients and magnetoviscous pinning. Langmuir. 2016;32(27):6967–6976.

[20] Katsikis G, Breant A, Rinberg A, et al. Synchronous magnetic control of water droplets in bulk ferrofluid. Soft Matter. 2018;14:681–692.

[21] Jamin T, Py C, Falcon E. Instability of the origami of a ferrofluid drop in a magnetic field. Phys Rev Lett. 2011;107:204503.

[22] Anjos PHA, Carvalho GD, Lira SA, et al. Wrinkling and folding patterns in a confined ferrofluid droplet with an elastic interface. Phys Rev E. 2019; 99:022608.

[23] Varma VB, Ray A, Wang Z, et al. Control of ferrofluid droplets in microchannels by uniform magnetic fields. IEEE Magn Lett. 2016;7:1–5.

[24] Chen CY, Hsueh HC, Wang SY, et al. Self-assembly and novel planetary motion of ferrofluid drops in a rotational magnetic field. Microfluid Nanofluidics. 2014;18.

[25] Cunha LHP, Siqueira IR, Oliveira TF, et al. Field-induced control of ferrofluid emulsion rheology and droplet break-up in shear flows. Phys Fluids. 2018; 30(12):122110.

[26] Zhu GP, Nguyen NT, Ramanujan RV, et al. Nonlinear deformation of a ferrofluid droplet in a uniform magnetic field. Langmuir. 2011;27(24):14834–14841.

[27] Ghaffari A, Hashemabadi SH, Bazmi M. Cfd simulation of equilibrium shape and coalescence of ferrofluid droplets subjected to uniform magnetic field. Colloids Surf A Physicochem Eng Asp. 2015; 481:186 – 198.

[28] Afkhami S, Tyler AJ, Renardy Y, et al. Deformation of a hydrophobic ferrofluid droplet suspended in a viscous medium under uniform magnetic fields. J Fluid Mech. 2010;663:358–384.

[29] Ghaffari A, Hashemabadi SH. Parameter study and CFD analysis of head on collision and dynamic behavior of two colliding ferrofluid droplets. Smart Mater Struct. 2017;26(3):035010.

[30] QIAN J, LAW CK. Regimes of coalescence and separation in droplet collision. J Fluid Mech. 1997; 331:59–80.

[31] Rosensweig, RE. *Ferrohydrodynamics*. Dover Books on Physics. Dover Publications. 2013.

[32] Mika Latikka and Matilda Backholm and Jaakko VI Timonen and Robin HA Ras. Wetting of ferrofluids: Phenomena and control. Current Opinion in Colloid & Interface Science. 2018;36:118 – 129. Wetting and Spreading.

[33] Kawun P, Leahy S, Lai Y. A thin pdms nozzle/diffuser micropump for biomedical applications. Sens Actuators A Phys. 2016;249:149 – 154.

[34] Afkhami S, Renardy Y, Renardy M, et al. Field-induced motion of ferrofluid droplets through immiscible viscous media. J Fluid Mech. 2008; 610:363–380.

[35] Zhu GP, Nguyen NT, Ramanujan RV, et al. Nonlinear deformation of a ferrofluid droplet in a uniform magnetic field. Langmuir. 2011;27(24):14834–14841.

[36] Afkhami S, Renardy Y, Renardy M, et al. Numerical modeling of ferrofluid droplets in magnetic fields. AIP Conf Proc. 2008;1027(1):884–886.

[37] Canny J. A computational approach to edge detection. IEEE Trans Pattern Anal Mach Intell. 1986; 8(6):679–698.

Address correspondence to:
Hamid Marvi
School for Engineering of Matter Transport & Energy

Arizona State University
551 E. Tyler Mall, Room ERC 365
PO Box 876106
Tempe, AZ 85287-6106
USA

E-mail: hmarvi@asu.edu

Supplementary Information for

A Shapeshifting Ferrofluidic Robot

Reza J. Ahmed, Mahdi Ilami, Joseph Bant, Borhan Beigzadeh, Hamid Marvi

Corresponding Author: Hamid Marvi
E-mail: hmarvi@asu.edu

This PDF file includes:

Supplementary text
Figs. S1 to S2
Caption for Movie S1
References for SI reference citations

Other supplementary materials for this manuscript include the following:

Movie S1

Supporting Information Text

The ferrofluid is assumed to be a magnetized body described by a magnetic moment $\mathbf{M}$. As such, the magnetic moment is dependent on the applied field and can rotate with respect to the body and its magnitude can vary greatly with changes in the applied field. The torque on the magnet is expressed as such:

$$\boldsymbol{T} = \mathbf{M} \times \mathbf{B} \quad [1]$$

where $\mathbf{B}$ is the applied magnetic field's flux density at the location of $\mathbf{M}$ (1). The torque tends to align the magnetic moment with the applied field. The magnetic force is expressed as:

$$\boldsymbol{F} = (\mathbf{M} \cdot \nabla)\mathbf{B} \quad [2]$$

Since there is no electric current flowing through the region occupied by the body, Maxwell's equations provide the constraint $\nabla \times \mathbf{B} = \mathbf{0}$. This allows us to express Eq. (2), in this form:

$$\boldsymbol{F} = \begin{bmatrix} \frac{\partial \mathbf{B}}{\partial x} & \frac{\partial \mathbf{B}}{\partial y} & \frac{\partial \mathbf{B}}{\partial z} \end{bmatrix}^T \mathbf{M} \quad [3]$$

With the static arrangement of electromagnets, each electromagnet creates a magnetic field throughout the workspace that can be pre-calculated. At any point $\boldsymbol{P}$ in the workspace, the magnetic field due to actuating a given electromagnet can be expressed by the vector $\boldsymbol{B}_e(\boldsymbol{P})$, whose magnitude varies linearly with the current through the electromagnet and as such can be described as a unit-current vector multiplied by a scalar current value:

$$\boldsymbol{B}_e(\boldsymbol{P}) = \tilde{\boldsymbol{B}}_e(\boldsymbol{P}) i_e \quad [4]$$

Due to the design of our setup, it can be assumed that the magnetic field at a point in the workspace is the sum of the contribution of the individual electromagnetic coils. This linear summation of fields can be expressed as follows:

$$\mathbf{B}(\boldsymbol{P}) = \begin{bmatrix} \tilde{\boldsymbol{B}}_1(\boldsymbol{P}) & \cdots & \tilde{\boldsymbol{B}}_n(\boldsymbol{P}) \end{bmatrix} \begin{bmatrix} i_1 \\ \vdots \\ i_n \end{bmatrix} = \boldsymbol{\beta}(\boldsymbol{P}) I \quad [5]$$

Considering (1), (3), and (5), the magnetic torque and forces on the ferrofluid can be expressed as follows:

$$\begin{bmatrix} \boldsymbol{T} \\ \boldsymbol{F} \end{bmatrix} = \begin{bmatrix} Sk(\mathbf{M})\boldsymbol{\beta}(\boldsymbol{P}) \\ \mathbf{M}^T \boldsymbol{\beta}_x(\boldsymbol{P}) \\ \mathbf{M}^T \boldsymbol{\beta}_y(\boldsymbol{P}) \\ \mathbf{M}^T \boldsymbol{\beta}_z(\boldsymbol{P}) \end{bmatrix} \begin{bmatrix} i_1 \\ \vdots \\ i_n \end{bmatrix} = \boldsymbol{A}_{T,F}(\mathbf{M}, \boldsymbol{P}) I \quad [6]$$

That is, for each ferrofluid pose, the n electromagnet currents are mapped to a torque and force through a $6 \times n$ actuation matrix $A_{T,F}(\mathbf{M}, \boldsymbol{P})$. For a desired torque/force vector, the choice of currents closest to the desired torque/force value can be found using the pseudo-inverse (1).

$$I = \boldsymbol{A}_{T,F}(\mathbf{M}, \boldsymbol{P})^{\dagger} \begin{bmatrix} \boldsymbol{T}_{\text{desired}} \\ \boldsymbol{F}_{\text{desired}} \end{bmatrix} \quad [7]$$

.

Because the ferrofluid can align with the applied field unimpeded, rather than explicitly controlling the torque one can control the field to the desired orientation and then explicitly control the force of the ferrofluid

$$\begin{bmatrix} \mathbf{B} \\ \boldsymbol{F} \end{bmatrix} = \begin{bmatrix} \boldsymbol{\beta}(\boldsymbol{P}) \\ \mathbf{M}^T \boldsymbol{\beta}_x(\boldsymbol{P}) \\ \mathbf{M}^T \boldsymbol{\beta}_y(\boldsymbol{P}) \\ \mathbf{M}^T \boldsymbol{\beta}_z(\boldsymbol{P}) \end{bmatrix} \begin{bmatrix} i_1 \\ \vdots \\ i_n \end{bmatrix} = \boldsymbol{A}_{B,F}(\mathbf{M}, \boldsymbol{P}) I \quad [8]$$

The current I is then set as follows:

$$I = \boldsymbol{A}_{B,F}(\mathbf{M}, \boldsymbol{P})^{\dagger} \begin{bmatrix} \mathbf{B}_{\text{desired}} \\ \boldsymbol{F}_{\text{desired}} \end{bmatrix} \quad [9]$$

In this case, the ferrofluid will align with the applied field under open-loop control. If the direction of $\mathbf{B}$ does not change quickly, it is reasonable to assume that $\mathbf{M}$ is always aligned with $\mathbf{B}$, which means that one must only estimate the magnitude of $\mathbf{M}$ and measure the ferrofluid's position $\boldsymbol{P}$.

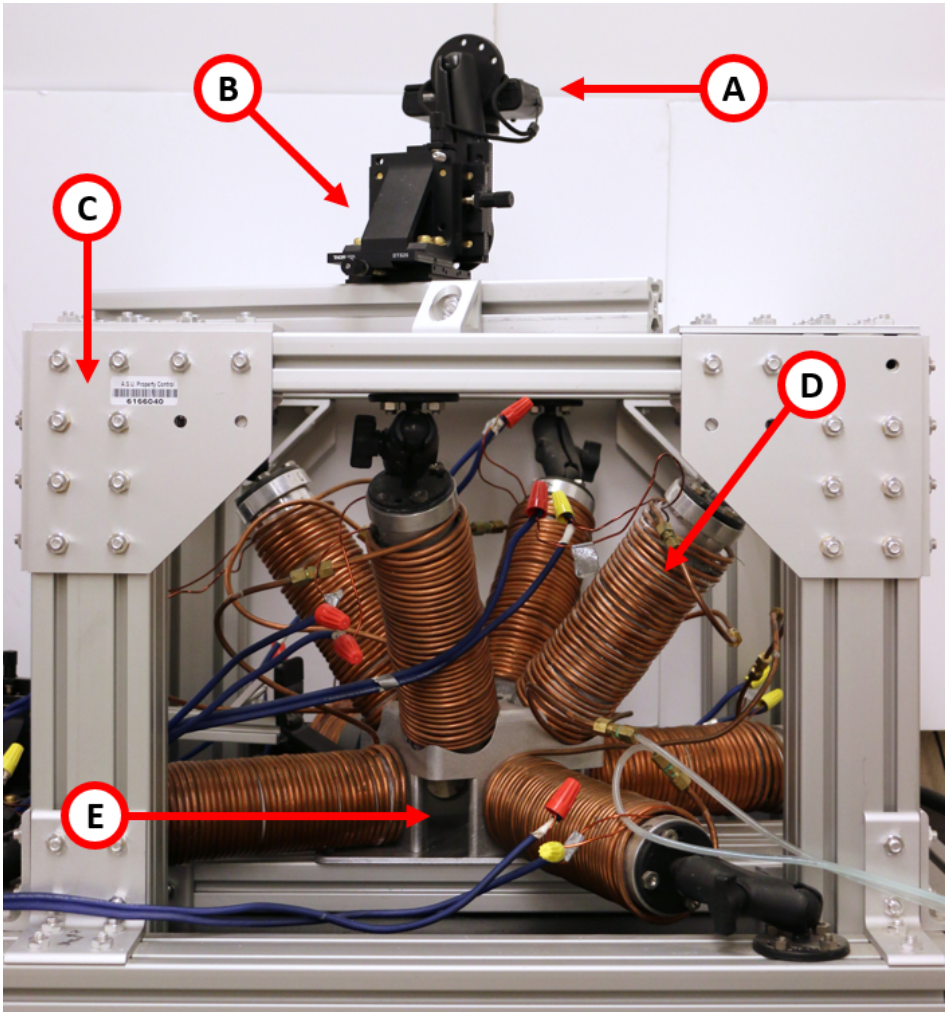

Fig. S1. Electromagnetic field generation system. A) Sony RX100 v camera for obtaining position and shape feedback for controllers. B) Thorlabs DTS25 translational stage for acute adjustment of camera view. C) Aluminum frame made of a combination of 8020 parts and custom machined parts. D) Electromagnetic coil wrapped with copper tubes that circulate chilled water, regulating temperature. E) Access portal for insertion of the work space cube into the center of the electromagnetic coil system.

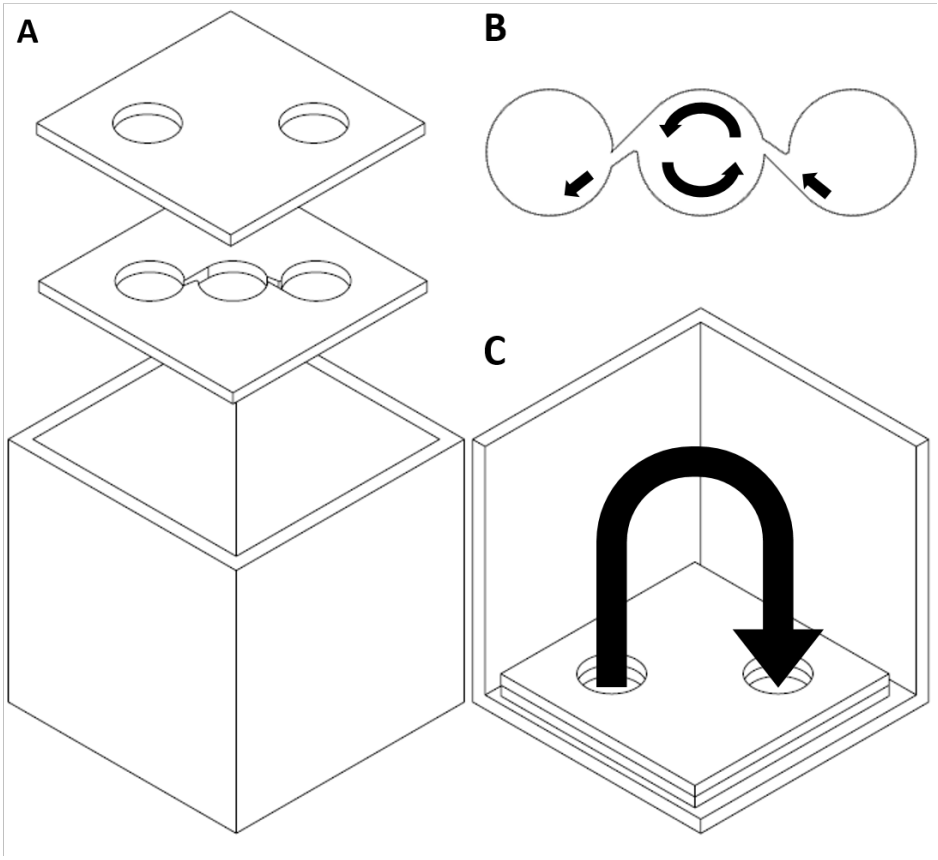

Fig. S2. A) Exploded view of pump assembly. The lower workspace-box and two pump layers are laser cut from acrylic sheets. B) Detail view of the pump structure. Between each chamber is a nozzle and diffuser to guide flow in one direction based on the design of Kawun *et al.* (2). C) Break out view of pump assembly with arrow representing direction of return flow.

Movie S1. Ferromoebot: A Ferrofluidic Amoeba-Inspired Robot. This video contains footage of the quantitative experiments: stretch angle control, stretch length control, and combined position and shape lemniscate experiments for both 4 and 8 coil control. Additionally, it contains video footage of the bio-inspired maneuver experiments: splitting and recombining, squeezing through a channel, particle engulfment and manipulation, and rotational pumping experiments.

References

1. MP Kummer, et al., Octomag: An electromagnetic system for 5-dof wireless micromanipulation. *IEEE Transactions on Robotics* **26**, 1006–1017 (2010).
2. P Kawun, S Leahy, Y Lai, A thin pdms nozzle/diffuser micropump for biomedical applications. *Sensors Actuators A: Phys.* **249**, 149 – 154 (2016).